

Coupling between phonon and short-range spin correlations in frustrated spinel $LiFeCr_4O_8$

Xiang Li(李想), Wei Ren(任玮), Bo Zhang(张博), Yan-Zhen Cai(蔡焱桢), Zhi-Wei Li(李志伟), Jianting Ji(籍建葶), Feng Jin(金峰), Anmin Zhang(张安民), and Qingming Zhang(张清明)
Citation: Chin. Phys. B, 2025, 34 (**11**): 117801. DOI: 10.1088/1674-1056/ade4b4
http://cpb.iphy.ac.cn; http://iopscience.iop.org/cpb

What follows is a list of articles you may be interested in

Stokes/anti-Stokes Raman spectroscopy of $Al_{0.86}Ga_{0.14}N$ semiconductor alloy

Yuru Lin(林玉茹), Yu Li(李宇), Binbin Wu(吴彬彬), Jingyi Liu(刘静仪), Ruiang Guo(郭睿昂), Yangbin Wang(王扬斌), Qiwei Hu(胡启威), and Li Lei(雷力)
Chin. Phys. B, 2025, 34 (**5**): 057802. DOI: 10.1088/1674-1056/adb67d

Intensity enhancement of Raman active and forbidden modes induced by naturally occurred hot spot at GaAs edge

Tao Liu(刘涛), Miao-Ling Lin(林妙玲), Da Meng(孟达), Xin Cong(从鑫), Qiang Kan(阚强), Jiang-Bin Wu(吴江滨), and Ping-Heng Tan(谭平恒)
Chin. Phys. B, 2025, 34 (**1**): 017801. DOI: 10.1088/1674-1056/ad9ff9

Surface-enhanced fluorescence and application study based on Ag-wheat leaves

Hongwen Cao(曹红文), Liting Guo(郭立婷), Zhen Sun(孙祯), Tifeng Jiao(焦体峰), and Mingli Wang(王明利)
Chin. Phys. B, 2022, 31 (**3**): 037803. DOI: 10.1088/1674-1056/ac1f0d

High-pressure Raman study of osmium and rhenium up to 200 GPa and pressure dependent elastic shear modulus C_{44}

Jingyi Liu(刘静仪), Yu Tao(陶雨), Chunmei Fan(范春梅), Binbin Wu(吴彬彬), Qiqi Tang(唐琦琪), and Li Lei(雷力)
Chin. Phys. B, 2022, 31 (**3**): 037801. DOI: 10.1088/1674-1056/ac1eff

Magnetic polaron-related optical properties in Ni(II)-doped CdS nanobelts: Implication for spin nanophotonic devices

Fu-Jian Ge(葛付建), Hui Peng(彭辉), Ye Tian(田野), Xiao-Yue Fan(范晓跃), Shuai Zhang(张帅), Xian-Xin Wu(吴宪欣), Xin-Feng Liu(刘新风), and Bing-Suo Zou(邹炳锁)
Chin. Phys. B, 2022, 31 (**1**): 017802. DOI: 10.1088/1674-1056/ac0782

Coupling between phonon and short-range spin correlations in frustrated spinel $LiFeCr_4O_8$

Xiang Li(李想)[1,†], Wei Ren(任玮)[1,†], Bo Zhang(张博)[1], Yan-Zhen Cai(蔡焱桢)[1], Zhi-Wei Li(李志伟)[1], Jianting Ji(籍建葶)[2], Feng Jin(金峰)[2], Anmin Zhang(张安民)[1,‡], and Qingming Zhang(张清明)[2,1]

[1] *School of Physical Science and Technology, Key Laboratory of Quantum Theory and Applications of MoE, Lanzhou University, Lanzhou* 730000, *China*
[2] *Beijing National Laboratory for Condensed Matter Physics, Institute of Physics, Chinese Academy of Sciences, Beijing* 100190, *China*

(Received 15 April 2025; revised manuscript received 4 June 2025; accepted manuscript online 16 June 2025)

Spin–phonon coupling is important in chromate spinel oxides ACr_2O_4, but its role in $LiFeCr_4O_8$ is not well understood. In this paper, we employ Raman scattering and first-principles phonon calculations to study this material. Ten out of 13 Raman-active modes are well assigned. Notably, no phonon splitting is observed across the structural phase transition due to the remarkably small Grüneisen constants. This observation, in conjunction with the structural data, provides compelling evidence that the structural phase transition in $LiFeCr_4O_8$ is primarily driven by the spin-driven Jahn–Teller effect. Interestingly, some Raman modes (at 207 cm^{-1}, 306 cm^{-1} and 462 cm^{-1}) exhibit unusual linewidth behavior across the temperature range investigated. Furthermore, the Raman spectra in different phases show no magnetic field dependence. These results suggest that phonons couple with short-range spin correlations, offering insights into how spin and lattice degrees of freedom interact in frustrated systems.

Keywords: Raman scattering, phonons, first-principles phonon calculations, magnetic materials

PACS: 78.30.–j, 63.20.–e, 63.20.dd, 74.25.Kc

DOI: 10.1088/1674-1056/ade4b4 **CSTR:** 32038.14.CPB.ade4b4

1. Introduction

In geometrically frustrated systems, spins on a lattice of polygons or polyhedra with an odd number of sides experience antiferromagnetic coupling with each other, making it impossible to simultaneously satisfy all interactions with neighboring spins. These systems provide a solid foundation for exploring exotic physical properties.[1–5] Chromate spinel ACr_2O_4 is a typical example of such a frustrated system.[6] In these materials, frustration arises from the antiferromagnetic nearest-neighbor interactions $J_{Cr–Cr}$, suppressing long-range spin order. However, strong spin–phonon coupling can relieve this frustration, usually accompanied by a structural phase transition, known as the spin-driven Jahn–Teller effect.[7–9] This removes the spin degeneracy of the ground state, and consequently a long-range spin order can develop, as observed in $ZnCr_2O_4$ and $CdCr_2O_4$.[9–11] When magnetic atoms occupy the A-site and $J_{A–Cr}$ is large enough to overcome frustration, the system will exhibit a higher Néel temperature. If the A-site magnetic ions in a cubic spinel structure exhibit orbital degeneracy, the system undergoes a tetragonal distortion above the Néel temperature driven by the cooperative Jahn–Teller effect. Additionally, a monoclinic structural transition occurs at the magnetic transition temperature.[12,13]

Compounds with two types of A-site atoms, such as $LiACr_4O_8$ (A = Ga, In, Fe), exhibit more interesting behaviors.[14–18] Ordering between Li and A atoms exerts different chemical pressures on the Cr_4 pyrochlore network, altering Cr–Cr bond lengths. This effect results in the formation of a 'breathing' pyrochlore structure, which could host the hedgehog spin textures (magnetic monopoles) proposed by Aoyama and Kawamura.[19] Furthermore, this ordering breaks the inversion symmetry of the original spinel structure ($Fd\bar{3}m$), turning it into a lower-symmetry space group ($F\bar{4}3m$).

As shown in $ZnCr_2O_4$, spin–lattice coupling always plays a crucial role in spinel compounds. Saha *et al.*[16] observed anormal Raman modes in $LiFeCr_4O_8$ near the magnetic ordering temperature T_N, spin-gap transition T_{SG} and magnetostructural and structural transition T_{MS}. Recently, Okamoto *et al.*[17] reported a significant volume increase in $LiFeCr_4O_8$ at T_{MS} under a magnetic field up to 9 T. To better understand the nature of this coupling in $LiFeCr_4O_8$, detailed Raman scattering is essential as it provides a powerful tool for probing the lattice, spin and their interactions.

In this paper, we used Raman scattering and first-principles phonon calculations to investigate the lattice dynamics and spin–phonon coupling in $LiFeCr_4O_8$. Ten of 13 Raman-active modes were assigned, and their frequencies agree with theoretical predictions. Furthermore, phonon mode splitting expected during the structural phase transition was not observed due to the small Grüneisen constants. Com-

[†]These authors contributed equally to this work.
[‡]Corresponding author. E-mail: amzhang@lzu.edu.cn

© 2025 Chinese Physical Society and IOP Publishing Ltd. All rights, including for text and data mining, AI training, and similar technologies, are reserved.

bined with temperature-dependent x-ray diffraction (XRD), we concluded that the structural phase transition is driven by the spin-driven Jahn–Teller effect. Unlike previous studies, we did not observe any anomalies in the phonon frequencies near $T_N \sim 97$ K, $T_{SG} \sim 54$ K or $T_{MS} \sim 27$ K. Interestingly, the line widths of a T_2 mode at 207 cm^{-1}, an E mode at 306 cm^{-1} and an A_1 mode at 462 cm^{-1} are unusually broad, with the first two continuing to broaden as temperature decreases and exhibiting anomalies near the phase transition. However, the Raman spectra in different phases exhibit magnetic-field-independent behavior. These observations can be explained by the coupling between phonons and frustration-enhanced short-range spin correlations.

2. Method

A polycrystalline powder of $LiFeCr_4O_8$ was prepared using the conventional solid-state reaction technique.[18] Stoichiometric amounts of Li_2CO_3, Fe_2O_3 and Cr_2O_3 (all from Alfa Aesar, 99.99%)) were mixed, formed into pellet and then heated in air at 1050 °C for 15 h, followed by cooling at a rate of 50 °C/h to reach room temperature. The XRD data were collected by a Guinier camera (G670, HUBER) and analyzed using the FullProf suite.[20] The results confirmed the high quality of our samples. The magnetic behavior was measured by a superconducting quantum interference device under a magnetic field of 100 Oe.

Raman spectra were collected with a LABRAM HR Evolution spectrometer equipped with a 1800 lines/mm grating, a liquid-nitrogen-cooled charge-coupled device and a 473 nm laser. Temperature- and field-dependent Raman spectra were measured in a closed-cycle pulse-tube refrigerator (1.8–300 K, 0–9 T, attoDRY2100, attocube).

To determine the phonon modes of $LiFeCr_4O_8$, we conducted first-principles electronic structure calculations using the projector-augmented-wave method,[21] as implemented in the Vienna *Ab Initio* Simulation Package.[22–24] For the exchange–correlation potential, the Perdew–Burke–Ernzerhof generalized gradient approximation was adopted.[25] The kinetic energy cutoff of the plane-wave basis was set to 600 eV. A $11 \times 11 \times 11$ k-point mesh was employed for the Brillouin zone sampling. Gaussian smearing with a width of 0.05 eV was used around the Fermi surface. In the structural optimization, both the cell parameters and internal atomic positions were allowed to relax. The total energies were converged to less than 10^{-8} eV to achieve good self-consistency in the electronic step and the positions of the ions were relaxed toward the equilibrium position using the conjugate gradient algorithm until the force acting on each atom was less than 0.002 eV/Å. The DFT $+U$ method[26] was used to take into account the electron correlation effects for the localized Fe/Cr 3d states in the spherically averaged approach with $U_{\text{eff}} = 4.0$ eV. The calculated lattice parameter $a = 8.27572$ Å is in good agreement with the experimental values.[16,18] After the equilibrium structure was obtained, the vibrational frequencies and polarization vectors at the center of the Brillouin zone were calculated using the density functional perturbation theory method.[27,28]

3. Results

At room temperature, $LiFeCr_4O_8$ exhibits a cubic crystal structure with space group $F\bar{4}3m$ (point group T_d). The symmetry analysis yields 13 Raman-active modes $\Gamma_R = 3A_1 + 3E + 7T_2$ at the Brillouin zone center Γ. Phonon modes can be assigned based on depolarization ratios, which are defined as the ratios of the intensities of scattered light polarized perpendicular to the plane to that polarized in the scattering plane $I_\perp/I_\parallel$.[29] Due to the presence of small single crystals with different orientations, the ratios can differ at different locations(see supplemental material Section 1). Therefore, three sites were selected for measurement. Figure 1 presents the polarized Raman spectra from site 1 above T_{MS}, with full data in Table 1. The results indicate that P^2, P^3 and P^5 can be categorized into one group, P^4, P^9 and P^{10} into another, and P^1, P^6, P^7 and P^8 into a third. Among these, P^6 exhibits a notable deviation in the depolarization ratio, possibly due to overlap with a mode from minor Cr_2O_3 impurities (see supplemental material Section 2).[30] Hence, the observed phonon modes can be classified into three categories, i.e., E, A_1 and T_2 modes. The remaining modes marked in red were not definitively assigned.

To relate observed peaks to the specific modes and atomic displacements, we conducted first-principles calculations. The theoretical results are summarized in Table 1, with atomic displacements of all optical phonon modes shown in supplemental material Section 3. The calculated frequencies show good agreement with experiments, except for the P^4 mode. Previous study has highlighted disparities in the calculated Cr–Cr distances in magnetic and non-magnetic environments for $LiGaCr_4S_8$.[31] The P^4 mode is associated with magnetic atoms, and the complex magnetic environment in $LiFeCr_4O_8$ may cause deviations between the calculations and experiments.

Figure 2(a) presents the temperature dependence of the Raman spectra, showing a smooth evolution with no additional peaks emerging. However, XRD patterns confirm a complete structural phase transition from $F\bar{4}3m$ to $I\bar{4}m2$ (see supplemental material Section 4). Symmetry analysis indicates 26 Raman-active modes in the $I\bar{4}m2$ phase: $\Gamma_R = 6A_1 + 3B_1 + 7B_2 + 10E$. In other words, seven T_2 modes in the cubic phase will split and some new modes will appear. This contradiction can be explained by the small Grüneisen constants.

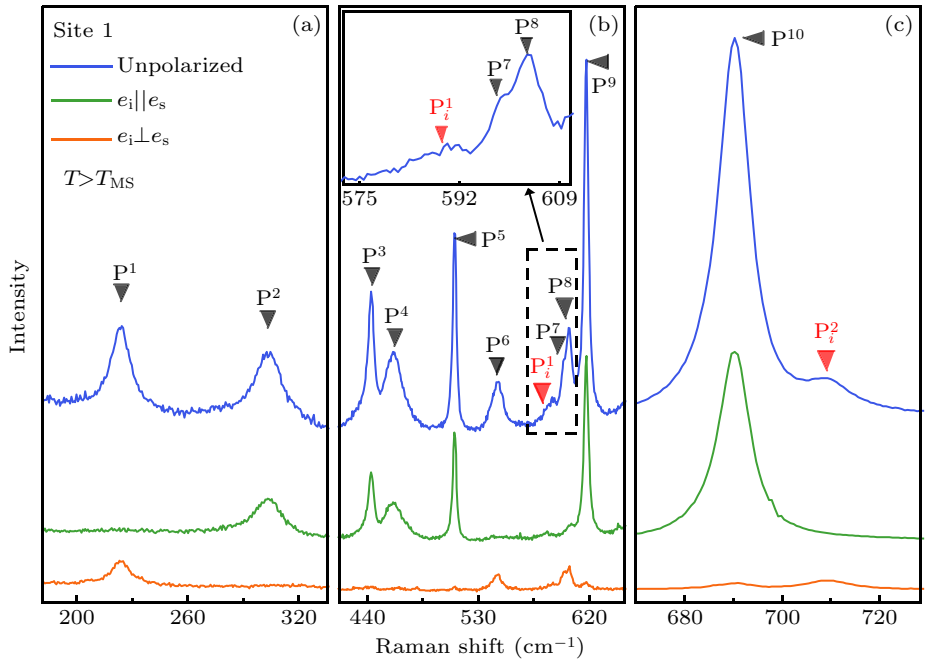


Fig. 1. Polarized Raman spectra of $LiFeCr_4O_8$ at site 1 above T_{MS}. The results from the other sites can be found in the supplemental material Section 1. e_i and e_s represent the polarizations of incident and scattered light, respectively. The assigned modes are labeled in black, and the unassigned modes are shown in red. The inset demonstrates that P^7 and P^8 remain distinguishable from each other.

Table 1. Assignments of Raman modes of $LiFeCr_4O_8$. The calculated phonon frequencies are in good agreement with experiments. Additionally, results from Ref. [32] are included. Moreover, the main atomic motions and depolarization ratio ρ measured at different sites are also presented here.

Symmetry	Calc. freq. (cm^{-1})	Main atom	Exp. freq. (4 K) (cm^{-1})	Exp. freq. (cm^{-1})[32]	Depolarization ratio ρ			Grüneisen parameter
					Site 1	Site 2	Site 3	
	491.49	Cr,O	462.78 (P^4)		0.016	0.233	0.006	0.011
A_1	624.31	O	619.96 (P^9)		0.039	0.218	0.062	3.5×10^{-4}
	690.85	O	694.45 (P^{10})		0.036	0.213	0.034	9.4×10^{-5}
	322.99	Cr,O	307.01 (P^2)		0.053	0.182	0.851	0.296
E	438.69	O	446.58 (P^3)		0.054	0.173	0.796	0.022
	520.2	O	512.68 (P^5)		0.027	0.179	0.764	2.9×10^{-3}
	226.64	Fe,O	226.99 (P^1)		12.817	2.884	2.482	–
	335.02	Li,Cr,O						
	446.29	Li		435				
T_2	478.3	Cr,O		495				
	542.27	Li,O	549.78 (P^6)	545	5.432	1.622	1.238	2.1×10^{-3}
	592.74	O	601.88 (P^7)	597	1.871	2.824	2.062	–
	606.1	O	606.75 (P^8)	635	2.403	2.166	1.534	–

In magnetic materials, the temperature dependence of phonon frequencies can be attributed to several factors: (i) lattice expansion/contraction, (ii) anharmonicity effects, (iii) renormalization of electronic states near the spin ordering temperature, and (iv) the spin–phonon contribution arising from the modulation of the exchange integral by lattice vibration.[33] The phonon frequency shift due to lattice expansion/contraction can be estimated by the Grüneisen law

$$\left(\frac{\Delta\omega_\alpha}{\omega_\alpha}\right)_{\text{latt}} = -\gamma_\alpha\left(\frac{\Delta V}{V}\right), \tag{1}$$

where ω_α is the frequency of the normal mode α, ΔV represents change in lattice volume and γ_α is the Grüneisen parameter of this mode, typically ranging from 0.1 to 1.8 in spinel ferrites.[34–36] At low temperatures, anharmonic effects are negligible, and the smooth evolution of phonon frequencies across the magnetic phase transition indicates minimal contributions from spin–phonon or electronic effects. Thus, lattice expansion/contraction dominates the frequency shift. As depicted in Fig. 2(b), the lattice volume follows a nearly exponential temperature dependence due to thermal expansion above T_{MS}, represented by the formula[37]

$$V(T) = V_{T_r}\exp\left[\alpha_0\left(T-T_r\right)+\alpha_1\left(T^2-T_r^2\right)\right], \tag{2}$$

where α_0 and α_1 are constants and V_{T_r} represents the volume at reference temperature T_r 298 K. According to Eqs. (2) and (3), we have estimated the Grüneisen constants at 28 K, and the values are listed in Table 1.

At low temperatures, $LiFeCr_4O_8$ undergoes a transition from a cubic structure to an orthogonal structure due to com-

pression along the c-axis. At 4 K, the volume is $V = 2aac \approx 564.53$ Å^3, whereas at 28 K, it becomes $V = ccc \approx 564.96$ Å^3, indicating a relative volume change of $\Delta V/V \approx 0.0761\%$ (see supplemental material Section 4). According to Eq. (1), the frequency shift from 4 K to 28 K exhibits minimal change, remaining within experimental error. Thus, no peak splitting is observed during the structural phase transition.

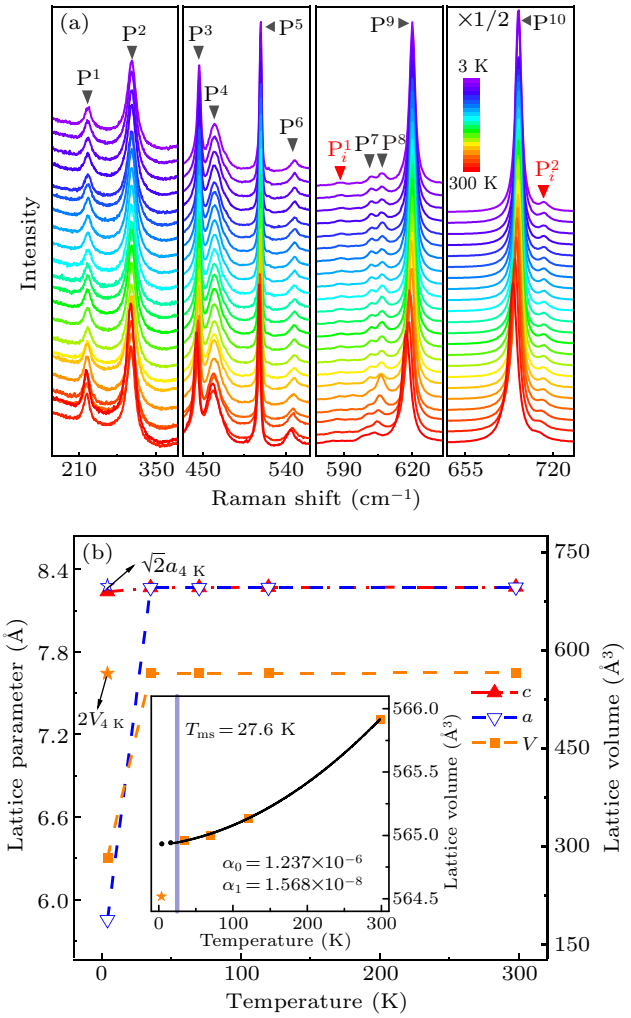


Fig. 2. (a) Temperature-dependent Raman spectra of $LiFeCr_4O_8$. (b) Lattice parameters (left axis) and volumes (right axis) of $LiFeCr_4O_8$ as a function of temperature. Yellow and blue stars represent $2V$ and $\sqrt{2}a$, respectively. The inset displays the variation of lattice volume with temperature, fitted to an exponential model, with α_0 and α_1 as the fitting parameters.

We extracted the temperature dependence of frequencies and line widths for eight relatively strong peaks. These modes fall into two groups, one being so-called normal modes. Their frequencies and line widths vary smoothly with temperature, as shown in Figs. 3(a)–3(f), and are well explained by an anharmonic phonon decay process[38,39]

$$\omega = \omega_0 - C\left(1 + \frac{2}{\exp(\hbar\omega_0/2k_BT) - 1}\right), \tag{3}$$

where ω_0, k_B and C are the phonon frequency extrapolated to 0 K, the Boltzmann constant and a fitting constant which represents the coupling strength between phonons, respectively

$$\Gamma = \Gamma^0_{anh}\left(1 + \frac{2a}{\exp(\hbar\omega_0/2k_BT) - 1}\right), \tag{4}$$

where Γ^0_{anh} is the anharmonic phonon broadening extrapolated to 0 K, ω_0 is the phonon frequency at 0 K and a is an anharmonic constant. It is worth noting that our Raman results show some differences from those reported in Ref. [16]. Based on our structural and magnetic measurements, which are in good agreement with previous studies, we believe that this discrepancy is unlikely to originate from sample quality or composition. We also note that the mode assignment in that reference was not explicitly detailed, which led to a different fitting approach from ours. These factors may contribute to the variation in results, and further investigation may be needed to fully clarify the origin of the discrepancy.

The other group comprises the P^1 and P^2 modes, whose frequencies follow the expected anharmonic temperature dependence, while their linewidths, as shown in Figs. 3(g) and 3(h), deviate significantly from standard anharmonic behavior. This suggests an additional decay channel beyond normal phonon–phonon coupling. Since $LiFeCr_4O_8$ is a magnetic insulator, this channel is likely to relate to spin order. This is further confirmed by the fact that P^1 and P^2 modes exhibit anomalies near the magnetic phase transition. Thus, we performed magnetic field-dependent Raman scattering. None of the spectra, including P^1 and P^2, show any magnetic field-dependent behavior from 1.8 K to 150 K, as shown in Fig. 4.

Generally, the effects of magnetic fields on phonons can be categorized into two mechanisms: magnetostriction and spin–phonon coupling. Okamoto *et al.*[17] reported strong spin–lattice coupling in $LiFeCr_4O_8$, where a 9 T magnetic field induces a volume change of approximately 500 ppm at T_{MS}. Although Raman scattering is sensitive to changes in lattice volume, no significant phonon frequency shift was observed in our measurements, probably due to the small magnetic Grüneisen constants of the material. The magnetic Grüneisen constant γ_{me} is related to the thermal Grüneisen constant γ_{th} and the thermal expansion coefficient α by the relation[40] $\gamma_{me} \propto \alpha\gamma_{th}/B$. Based on previous data,[17] α reaches a maximum value of only 0.0544. Given the small value of γ_{th}, γ_{me} is also expected to be small, making the phonon frequency shift induced by magnetostriction negligible. This result does not contradict the occurrence of magnetostriction in the sample. The magnetic field may also influence spin–phonon coupling; however, no significant effect was observed. This seems to contradict the idea that P^1 and P^2 are coupled with spin order.

The anomalous behavior of P^1 and P^2 can be attributed to their interactions with short-range spin correlations, as previously discussed by Wakamura for ferrimagnetic $FeCr_2S_4$.[41] In magnetic materials, the total crystal potential comprises

a general non-magnetic potential U_0 and a magnetic potential U_m, modulated by exchange interactions via phonon displacement $\boldsymbol{u}$. The second derivative of U_m with respect to $\boldsymbol{u}$ introduces an additional harmonic force constant, while the third derivative couples phonon damping with the spin system. The phonon frequency shift at the Brillouin zone center is related to long-range spin order, whereas the FWHM broadening is mainly due to coupling between phonons at the Brillouin zone center, phonons at the Brillouin zone boundary and short-range spin order. Both frequency and line width evolve together with the spin correlations $\langle S_i \cdot S_j \rangle$

$$\langle S_m S_n \rangle \propto (\langle M^{\alpha} \rangle^2 + NkT\chi^{\alpha\alpha}), \tag{5}$$

here M^{α} represents the magnetization from long-range spin order, while $\chi^{\alpha\alpha}$ is the magnetic susceptibility matrix, reflecting short-range spin correlations. N denotes the number of magnetic ions per unit cell.

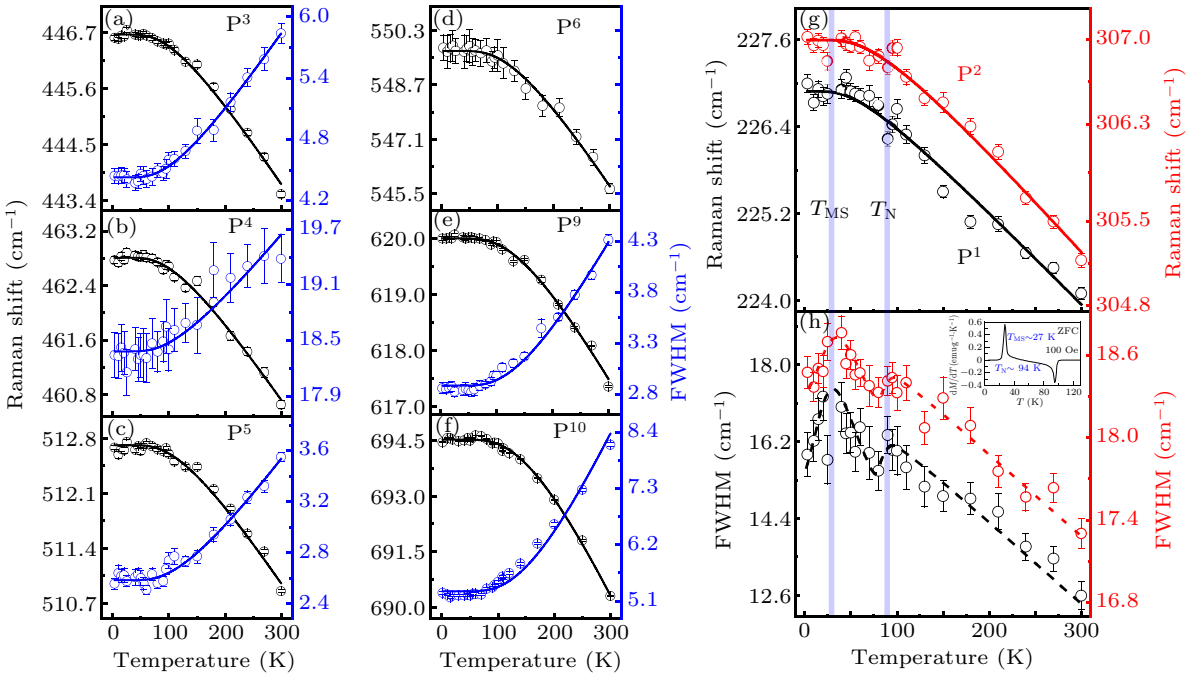


Fig. 3. The left panel presents the temperature dependence of the frequencies (left axis, black) and full width at half maximum (FWHM; right axis, blue) for P^3, P^4, P^5, P^6, P^9 and P^{10} modes of $LiFeCr_4O_8$ ((a)–(f)). The right panel shows the temperature dependence of (g) the frequencies and (h) the FWHM of P^1 (left axis, black) and P^2 (right axis, red) modes. The solid lines in (a)–(g) represent the fitted curves using Eqs. (3) and (4), and dashed lines in (h) serve as a guide to the eyes, showing the smoothing curve of the data. As shown in the inset, the phonon linewidths reach their maxima at T_{MS} and T_N.

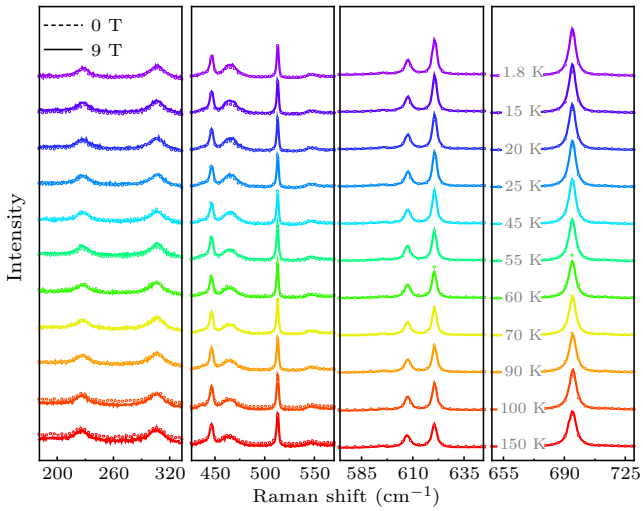


Fig. 4. Field-dependent Raman spectra of $LiFeCr_4O_8$ at temperatures ranging from 1.8 K to 150 K. The dashed lines represent spectra in the absence of a magnetic field, whereas the solid lines represent spectra under a magnetic field up to 9 T. The Raman spectra at 0 T and 9 T show negligible differences.

In this paper, the line widths of P^1, P^2 and P^4 are over three times broader than those of other phonons. These modes are linked to the magnetic atoms, indicating spin–phonon coupling. However, their frequency shifts are consistent with anharmonic phonon decay, suggesting that the second derivative of U_m is negligible. Among them, only the P^1 and P^2 modes exhibit anomalous temperature-dependent behavior. Their line widths broaden as temperature decreases, peaking near T_{MS} and T_N. This follows the behavior of spin correlation $\langle S_i \cdot S_j \rangle$, as shown in Fig. 3(h). In fact, $LiFeCr_4O_8$ exhibits strong frustration due to its pyrochlore network. The Curie–Weiss temperature θ obtained from the Curie–Weiss fitting ($\chi = C/T + \theta$) is greater than 1000 K, with a frustration index exceeding 18.[18] Spin fluctuations, enhanced by magnetic frustration, persist over a wide temperature range, including the region above T_{MS} covered in our experiments. Together with critical fluctuations associated with the transition, these

fluctuations lead to a broadening of the phonon linewidths as the temperature decreases. However, the short-range magnetic correlations are rapidly suppressed below T_{MS}.[16,18] As a result, the linewidths of these modes narrow with further cooling. Additionally, a 9 T magnetic field (at approximately 6 K) has little effect on the long-range spin order and spin fluctuations. Therefore, the Raman spectra exhibit magnetic-field-independent behavior.

Finally, we focus on the structural phase transition in $LiFeCr_4O_8$. In ACr_2O_4 compounds, structural transition can arise either from a conventional Jahn–Teller effect, driven by the lifting of orbital degeneracy through symmetry lowering, as exemplified by $FeCr_2O_4$, or from a spin-driven Jahn–Teller mechanism, where spin degeneracy is relieved by lattice distortion, as established in $ZnCr_2O_4$. In $LiFeCr_4O_8$, Fe is trivalent, unlike in $FeCr_2O_4$, where Fe^{2+} is Jahn–Teller active. Since Fe^{3+} lacks orbital degeneracy, a conventional Jahn–Teller effect is unlikely to be the driving force. This is further supported by temperature-dependent powder XRD data, which reveal only minimal changes in the bond lengths and angles of FeO_4 tetrahedra across the transition (see supplemental material Section 4), in contrast to compounds exhibiting Jahn–Teller distortion. These subtle variations indicate that the crystal field environment, and thus the electronic energy levels of the Fe ions, remain essentially unchanged. However, the Cr_4 tetrahedra distort during the transition, indicating a release of magnetic frustration. Moreover, the small Grüneisen constants extracted from our data suggest negligible changes in lattice potential energy. Instead, pronounced geometric frustration in this compound leads to substantial magnetic energy contributions above T_{MS}. During the magnetic structural transition, the release of spin frustration causes a significant reduction in magnetic potential energy, while the lattice potential energy is largely unaffected. Taken together, these findings exclude the conventional Jahn–Teller effect and point to a spin-driven Jahn–Teller mechanism as the origin of the structural transition.

4. Conclusion

In summary, we investigated spin–phonon coupling in $LiFeCr_4O_8$ by means of comprehensive Raman scattering. Through first-principles calculations and polarized Raman measurements, we successfully assigned 10 out of 13 Raman-active modes. Owing to the small Grüneisen constants, no phonon splitting was observed during the structural phase transition. Our results show that the temperature dependence of line widths of P^1 and P^2 modes deviates from conventional anharmonic behavior. Instead, a strong spin–phonon interaction, particularly short-range spin correlations, dominates the phonon decay process. This interaction is enhanced by spin frustration and might already exist above the magnetic transition temperature. Furthermore, structural analysis reveals that the structural phase transition in $LiFeCr_4O_8$ is governed by a spin-driven Jahn–Teller effect rather than the conventional Jahn–Teller effect. These results provide fundamental insights into the lattice dynamics of $LiFeCr_4O_8$ and are significant for understanding spin–phonon coupling in similarly frustrated systems.

Acknowledgements

This work was supported by the National Key Research and Development Program of China (Grant Nos. 2022YFA1402704 and 2022YFA1408302), the National Natural Science Foundation of China (Grant No. 12274186), the Strategic Priority Research Program of the Chinese Academy of Sciences (Grant No. XDB33010100), and the Synergetic Extreme Condition User Facility (SECUF). The authors are grateful for the support provided by the Supercomputing Center of Lanzhou University.

References

[1] Nilsen G J, Okamoto Y, Masuda T, Rodriguez-Carvajal J, Mutka H, Hansen T and Hiroi Z 2015 *Phys. Rev. B* **91** 174435
[2] Ramirez A 1994 *Annual Review of Materials Science* **24** 453
[3] Reimers J N 1992 *Phys. Rev. B* **45** 7287
[4] Moessner R and Ramirez A P 2006 *Physics Today* **59** 24
[5] Moessner R and Chalker J T 1998 *Phys. Rev. B* **58** 12049
[6] Kant C, Deisenhofer J, Tsurkan V and Loidl 2010 *J. Phys.: Conf. Ser.* **200** 032032
[7] Yamashita Y and Ueda K 2000 *Phys. Rev. Lett.* **85** 4960
[8] Tchernyshyov O, Moessner R and Sondhi S L 2002 *Phys. Rev. Lett.* **88** 067203
[9] Lee S H, Broholm C, Kim T H, Ratcliff W and Cheong S W 2000 *Phys. Rev. Lett.* **84** 3718
[10] Sushkov A B, Tchernyshyov O, II W R, Cheong S W and Drew H D 2005 *Phys. Rev. Lett.* **94** 137202
[11] Chung J H, Matsuda M, Lee S H, Kakurai K, Ueda H, Sato T J, Takagi H, Hong K P and Park S 2005 *Phys. Rev. Lett.* **95** 247204
[12] Bordács S, Varjas D, Kézsmárki I, Mihály G, Baldassarre L, Abouelsayed A, Kuntscher C A, Ohgushi K and Tokura Y 2005 *Phys. Rev. Lett.* **103** 077205
[13] Kocsis V, Bordács S, Varjas D, Penc K, Abouelsayed A, Kuntscher C A, Ohgushi K, Tokura Y and Kézsmárki I 2013 *Phys. Rev. B* **87** 064416
[14] Okamoto Y, Nilsen G J, Attfield J P and Hiroi Z 2013 *Phys. Rev. Lett.* **110** 097203
[15] Lee S, Do S H, Lee W J, Choi Y S, Lee M, Choi E S, Reyes A P, Kuhns P L, Ozarowski A and Choi K Y 2016 *Phys. Rev. B* **93** 174402
[16] Saha R, Dhanya R, Bellin C, Béneut K, Bhattacharyya A, Shukla A, Narayana C, Suard E, Rodríguez-Carvajal J and Sundaresan A 2017 *Phys. Rev. B* **96** 214439
[17] kamoto Y, Kanematsu T, Kubota Y, Yajima T and Takenaka K 2022 *J. Phys. Soc. Jpn.* **91** 023710
[18] Zhang B, Ren W, Yang S, Kuang Q, Li D, Liu X, Zhang A, Pang H, Tang L, Qiao L, Li F and Li Z 2023 *Phys. Rev. B* **108** 214401
[19] Aoyama K and Kawamura H 2019 *Phys. Rev. B* **99** 144406
[20] The programs of the FullProf suite can be found at https://www.ill.eu/sites/fullprof/.
[21] Blöchl P E 1994 *Phys. Rev. B* **50** 17953
[22] Kresse G and Hafner J 1993 *Phys. Rev. B* **47** 558
[23] Kresse G and Furthmüller J 1996 *Computational Materials Science* **6** 15
[24] Kresse G and Furthmüller J 1996 *Phys. Rev. B* **54** 11169
[25] Perdew J P, Burke K and Ernzerhof M 1996 *Phys. Rev. Lett.* **77** 3865
[26] Dudarev S L, Botton G A, Savrasov S Y, Humphreys C J and Sutton A P 1998 *Phys. Rev. B* **57** 1505

[27] Giannozzi P, de Gironcoli S, Pavone P and Baroni S 1991 *Phys. Rev. B* **43** 7231

[28] Gonze X and Lee C 1997 *Phys. Rev. B* **55** 10355

[29] Kobliska R J and Solin S A 1991 *Phys. Rev. B* **8** 756

[30] Gomes A S O, Yaghini N, Martinelli A and Ahlberg E 2017 *Journal of Raman Spectroscopy* **48** 1256

[31] Pokharel G, May A F, Parker D S, Calder S, Ehlers G, Huq A, Kimber S A J, Arachchige H S, Poudel L, McGuire M A, Mandrus D and Christianson A D 2018 *Phys. Rev. B* **97** 134117

[32] Tarte P and Preudhomme J 1973 *Spectrochimica Acta Part A: Molecular Spectroscopy* **29** 1301

[33] Granado E, García A, Sanjurjo J A, Rettori C, Torriani I, Prado F, Sánchez R D, Caneiro A and Oseroff S B 1999 *Phys. Rev. B* **60** 11879

[34] Wang Z, Schiferl D, Zhao Y and O'Neill H S C 2003 *Journal of Physics and Chemistry of Solids* **64** 2517

[35] Wang Z, Downs R T, Pischedda V, Shetty R, Saxena S K, Zha C S, Zhao Y S, Schiferl D and Waskowska A 2003 *Phys. Rev. B* **68** 094101

[36] Rahman S, Samanta S, Errandonea D, Yan S, Yang K, Lu J and Wang L 2017 *Phys. Rev. B* **95** 024107

[37] Fei Y and Ahrens T 1995 *Mineral physics and crystallography: a handbook of physical constants (American Geophysical Union)* **2** pp. 29–44

[38] Balkanski M, Wallis R F and Haro E 1983 *Phys. Rev. B* **28** 1928

[39] Gasanly N, Aydnl A, Özkan H and Kocabaş C 2002 *Materials Research Bulletin* **37** 169

[40] Pulvirenti P and Jiles D 1996 *IEEE Transactions on Magnetics* **32** 4785

[41] Wakamura K 1989 *Solid State Commun.* **71** 1033